Coded PPM and Multipulse PPM and Iterative Detection for Free-Space Optical Links

Fang Xu, Mohammad-Ali Khalighi, and Salah Bourennane

***Abstract*—Signal modulation has an important impact on the system performance in optical communication. Two attractive modulation schemes are pulse position modulation (PPM) and multipulse PPM (MPPM), which have the advantage of average energy efficiency and bandwidth efficiency, respectively. An important practical issue is to employ an efficient channel coding of reasonable (decoding) complexity adapted to these modulations. In this view, we consider the use of a classic binary convolutional code together with iterative soft demodulation and channel decoding at the receiver. In particular, we discuss the impact of bit-symbol mapping on the iterative receiver performance and provide design rules for optimal mapping in the case of MPPM.**

***Index Terms*—Channel coding; Iterative detection; Free-space optics; Multipulse PPM; Pulse position modulation**.

I. Introduction

Free-space optics (FSO), or optical wireless communication, is a promising solution for very high data rate point-to-point communication [1]. In practice, in FSO systems, we are faced with several practical problems, which may degrade the performance of an FSO link, particularly over ranges of the order of 1 km or longer [2–4]. In this paper, we assume that the transmitter and the receiver are fixed and perfectly aligned, and we consider clear atmosphere conditions. Even under such conditions, we are faced with atmospheric turbulence, also known as scintillation. The resulting channel fading, i.e., random fluctuations in both the amplitude and the phase of the received signal, can cause an important degradation in the quality of data transmission [5]. Under weak turbulence conditions, the system performance can be improved considerably by using channel coding [6–8]. However, in the cases of moderate to strong turbulence, channel coding alone is not sufficient to mitigate channel fading efficiently, and it should be used in combination with diversity techniques [8,9].

In this work, we mostly consider the conditions of weak turbulence. We assume that we do not have any source of diversity available: we use a monochromatic laser with a single beam at the transmitter and a single lens of very small size at the receiver, usually referred to as a point receiver. This assumption of the absence of any source of diversity allows us to focus on another interesting aspect with a view to improving the system performance, i.e., the signal modulation. The ON-OFF keying (OOK) modulation is commonly used in FSO systems owing to its simplicity. We are interested in more efficient modulation techniques that make a good compromise between complexity and performance. In this view, we consider in this paper pulse position modulation (PPM) and multipulse PPM (MPPM) and look for appropriate channel coding methods adapted to these modulations. The interest in PPM is that it is an average-energy efficient modulation [10]. Also, MPPM has the advantage of higher bandwidth efficiency, as compared with PPM [11].

In this work, we explain how to adapt a simple binary convolutional code to the case of Q-ary PPM or MPPM. As we will see, in order to efficiently correct demodulation errors, we perform iterative demodulation and channel decoding and, hence, benefit from the channel coding gain in signal demodulation. The receiver complexity remains reasonable, as compared with the case of nonbinary convolutional coding. We call this scheme BCID, standing for binary convolutional encoding with iterative detection. We study the system performance for PPM and MPPM modulations with an emphasis on the latter.

Note that a somewhat similar scheme, called serially concatenated pulse-position modulation (SCPPM), was recently proposed by Moision and Hamkins in [12,13]. This relatively high-complexity scheme is in

Manuscript received May 14, 2009; accepted July 6, 2009; published September 18, 2009 (Doc. ID 111396).

F. Xu (Fang.Xu@fresnel.fr), M.-A. Khalighi (Ali.Khalighi@fresnel.fr), and S. Bourennane (Salah.Bourennane@fresnel.fr) are with the École Centrale Marseille, Institut Fresnel, UMR CNRS 6133, Campus de Saint-Jérôme, 13397 Marseille Cedex 20, France.

Digital Object Identifier 10.1364/JOCN.1.000404

fact proposed for deep space communication with data rates of the order of megabits per second. Our BCID scheme can be considered a simplification of SCPPM. Our contribution is mainly in the extension of the BCID scheme to MPPM, as well as in discussing the choice of bit-symbol mapping and its effect on the performance of the iterative receiver. We provide, in particular, a design rule for signal mapping for MPPM.

Numerous works such as [14,15] have already considered the use of PPM for deep space communication while being based on a photon-counting receiver. We consider in this paper the context of terrestrial FSO systems used over ranges up to several kilometers. In most of these systems, the received photon flux is important enough to allow working with the beam intensity directly. Here, by FSO, we mean such systems and consider signal detection at the receiver based on the received light intensity. Note also that the assumption of the weak turbulence regime that we made is not restrictive: in the cases of moderate to strong turbulence, usually a relatively large lens is used at the receiver for aperture averaging [5]. This efficiently reduces the channel fading. Even with a sufficiently large aperture, the fading statistics mostly follow the log-normal distribution [9,16]. Thus, our study also applies to such cases.

The remainder of this paper is organized as follows. In Section II, we present our motivation behind choosing PPM and MPPM, as well as some already proposed channel coding solutions. The system model and general assumptions are presented in Section III. The iterative receiver is detailed in Section IV, whereas PPM mapping and soft demodulation are described in Section V. In Section VI, we extend our study to the case of MPPM and consider optimal bit-symbol mapping. Numerical results are presented in Section VII to compare the system performance for different coding and modulation schemes. Finally, Section VIII concludes the paper.

II. PPM AND CHANNEL CODING, STATE OF THE ART

Let us first explain our motivation for choosing PPM and MPPM, as well as their pros and cons. We also present a brief overview of the classic channel coding methods proposed so far.

A. Choice of Signal Modulation

Because of implementation complexity issues, most current FSO systems use intensity modulation with direct detection (IM/DD). It is shown in [17] that, for a classic optical channel under peak and average power constraints, a slotted binary modulation can nearly achieve the channel capacity. Furthermore, it is proved in [18] that, under such constraints, PPM can attain the near-optimum channel capacity. When performing hard signal detection at the receiver, PPM has the advantage that, in contrast to OOK, it does not require dynamic thresholding for optimal detection [19]. In this work, we perform soft signal detection at the receiver, however.

In the classic Q-ary PPM, a symbol corresponds to $B=\log_2 Q$ bits. We denote the symbol duration T_s and the slot (or chip) duration $T=T_s/Q$. The symbol duration is thus cut into Q time slots, and an optical pulse is sent in one of the Q slots. Figure 1(a) shows an example of Q-ary PPM with $Q=4$. For notational simplicity, hereafter, we denote the Q-ary PPM simply PPM or QPPM when we want to specify the modulation order. For the case of binary PPM (BPPM), i.e., $Q=2$, we use the BPPM notation. For QPPM, the required bandwidth increases linearly with Q. This does not cause a problem because FSO systems have a very large bandwidth available. However, the real problem with increasing Q is that, in practice, the required switching speed for the electronics increases. This means that more expensive devices must be used in the system. Moreover, the receiver synchronization becomes more difficult [10].

Since QPPM contains one pulse per Q slots, it has a duty cycle of $1/Q$ and a peak-to-average power ratio (PAPR) of Q. We can vary Q to make a flexible compromise between power efficiency and bandwidth efficiency. Nevertheless, a disadvantage of PPM is that for a given average transmission power, with increasing Q, the PAPR increases.

An interesting alternative to PPM is the MPPM, which has the advantage of reduced PAPR. In MPPM, we send w laser pulses among Q slots. Obviously, the case of $w=1$ corresponds to the conventional PPM. For MPPM that we denote w-QPPM, we have a duty cycle of w/Q and a PAPR of Q/w. As an example, we have shown in Fig. 1(b) the case of 2-4PPM, i.e., dual-pulse MPPM with $Q=4$. Another important advantage of MPPM over PPM is its higher bandwidth efficiency [11,20]. As explained above, from a practical point of view, the bandwidth efficiency is a parameter of criti-

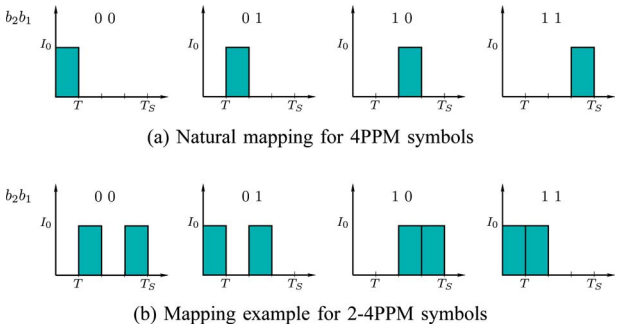

(a) Natural mapping for 4PPM symbols

(b) Mapping example for 2-4PPM symbols

Fig. 1. (Color online) Examples of PPM and MPPM symbols. I_0, transmitted light intensity in an ON slot.

cal importance in FSO systems. Performances of PPM and MPPM have been compared in several works [11,21]. When imposing a constraint on the peak power and nothing on the average power, MPPM outperforms PPM. When the constraint is imposed on the average power and nothing on the peak power, it is PPM that outperforms MPPM.

Some variations of PPM have also been developed for the wireless optical links, such as overlapping PPM and differential PPM. Overlapping PPM can be considered a special case of MPPM, where each symbol interval corresponds to NM slots with N ON-slots [14]. Differential PPM, on the other hand, has variable symbol duration, since each symbol begins just after the ON-slot of the preceding symbol. It, hence, necessitates stringent frame synchronization [14] and would not be suitable for commercial FSO systems.

B. Already Proposed Channel Coding Solutions

A number of coding techniques, including convolutional codes, Reed-Solomon (RS) codes, and turbocodes (TCs) have been proposed so far for QPPM. The classic binary convolutional codes and TCs were proposed in [22–25]. The main drawback of these solutions is that binary codes are not suitable for use with Q-ary symbols in the sense that they are not efficient for correcting demodulator output errors. Nonbinary codes are more appropriate [18]; however, their decoding complexity can be prohibitively large for a practical implementation in a gigabit-per-second FSO system. RS codes are appropriate from this point of view: an (n,k) RS code is naturally matched to Q-ary PPM by choosing $n=Q-1$ [26]. RS codes have also been considered for the case of MPPM [27]. Concatenated convolutional and RS codes were considered in [28]. However, the performance improvement by RS coding is not considerable because of hard RS decoding that is usually performed at the receiver; soft RS decoding is computationally too complex and is rarely implemented.

III. System Model and Assumptions

At the transmitter, the encoded information bits are transformed into symbols according to the modulation. We let I_0 denote the transmitted light intensity in an ON PPM slot, and I the corresponding received intensity. With the channel fading coefficient denoted h, we have, in fact, $I=hI_0$. At the receiver, the corresponding electrical signal after optical/electrical conversion is

$$r = \eta h I_0 + n, \tag{1}$$

where η is the optical/electrical conversion efficiency assumed to be unity for simplicity. Also, n is the sum of thermal, dark, and shot noise. We assume that the receiver is thermal noise limited and model n as a zero-mean Gaussian additive random process, independent of the received signal intensity I. Note that for an OFF PPM slot, Eq. (1) reduces to $r=n$.

Based on r, we perform soft signal demodulation and channel decoding. Soft information is considered in the form of the logarithmic likelihood ratio (LLR). We leave the details on this part to Section V. We assume perfect time synchronization of the system. Also, we assume that there is no spreading of the signal intensity across the slots of PPM symbols. This means that the signal corresponding to each time slot is independent of those of the other slots. In other words, we assume that we do not have any interslot interference.

We use the gamma–gamma ($\Gamma\Gamma$) model for the fade statistics. This model can be adapted to any turbulence conditions by setting two parameters, α and β, which are the effective numbers of large- and small-scale eddies of the scattering environment, respectively, and depend on the Rytov variance [5]. We consider here the classic plane wave propagation model, which is valid for relatively long-range applications, as well as turbulent eddies of zero inner scale. A normalized channel is considered, i.e., $E\{I\}=1$. Channel time variations are considered according to the theoretical quasi-static (*frozen*) model, where channel fading is constant over the duration of a frame of symbols, changing to a new independent value from one frame to the next.

IV. Iterative Demodulation and Decoding

As explained previously, we use a classic binary convolutional code at the transmitter. A binary code cannot efficiently correct the demodulator output errors in the case of using a Q-ary modulation, however. So, in order to improve the receiver performance, we use the decoder soft outputs to refine the demodulator's decisions. By performing iterative demodulation and decoding, we would hopefully obtain the same robustness as if we had used a nonbinary code, while having much less receiver complexity. We were inspired by the idea that is used in turbo-equalization or turbo-detection [29,30]. For the reason that will be explained later, at the transmitter we need to perform interleaving on the encoded bits before bit-symbol mapping.

The block diagram of the proposed receiver is shown in Fig. 2. We perform soft-input soft-output (SISO) demodulation and decoding. The former is based on the maximum *a posteriori* criterion and the latter on the maximum likelihood criterion using the soft output Viterbi algorithm (SOVA). Note that we use the words

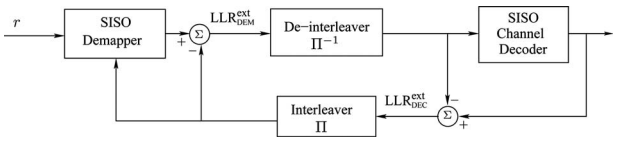

Fig. 2. Block diagram of the iterative receiver. $\mathrm{LLR}^{\mathrm{ext}}_{\mathrm{DEM}}$ and $\mathrm{LLR}^{\mathrm{ext}}_{\mathrm{DEC}}$, extrinsic soft values at the demapper and the channel decoder, respectively.

"demodulator" and "demapper" interchangeably. At the first iteration, the demapper calculates bit-level LLRs on the transmitted (coded) bits by using the received signal samples r. The demapper output LLRs are then fed to the SISO decoder that provides at its output LLRs on the coded bits. In the second iteration, the decoder output extrinsic LLRs are fed to the demodulator to help it refine the LLR calculation. The demodulator then provides the extrinsic LLRs to the decoder, and so on. After a few iterations, we obtain practically no improvement, i.e., we attain the convergence. Decision making on the transmitted bits can then be done by using the *a posteriori* LLRs at the decoder output. Note that passing extrinsic soft values between the two main blocks instead of *a posteriori* values ensures the proper convergence of the receiver.

An important parameter is the interleaver (or equivalently, the deinterleaver). The deinterleaver in Fig. 2 has the task of decorrelating the demapper outputs. In fact, the maximum likelihood decoding of the convolutional code is optimal when input errors to the decoder are uncorrelated. The receiver performance after convergence depends on the interleaver design. Here, we consider pseudorandom interleaving of large enough size.

As mentioned in Section I, a similar scheme, called SCPPM, was proposed in [12,13] for deep space communication applications. In the SCPPM scheme, the information bits are first encoded by using an *outer code*, which is a binary convolutional code [12,31]. Then, after interleaving, they are passed through an *inner encoder*, a combination of a bit-accumulator and a PPM modulator, called accumulated PPM. The use of low-density-parity-check codes instead of convolutional codes is considered in [32]. Later, single-parity-check codes were applied to SCPPM in [33]. The difference from our scheme comes essentially from the bit-accumulator. The use of accumulated PPM allows the iterative decoder to obtain better performances [31] but increases its complexity. The BCID scheme that we consider here has a reduced complexity and is more suitable for a gigabit-per-second FSO system.

V. Soft Demapping of PPM Symbols

In this section, we provide details on mapping and soft demapping of PPM symbols.

A. Q-ary PPM Mapping

The interleaved coded bits are grouped into sub-blocks of $B=\log_2 Q$ bits, $(b_B, b_{B-1}, \ldots, b_1)$, and fed to the PPM modulator. Let $\boldsymbol{x}=(x_1, x_2, \ldots, x_Q)$ represent the transmitted symbol corresponding to the Q slots of a PPM symbol. We sometimes refer to $\boldsymbol{x}$ as a *slot-word*. As we assumed a channel free of interslot interference, the method of mapping the bits to symbols has no effect on the system performance. Therefore, we consider here the simple natural mapping. By this mapping, the position of the optical pulse in $\boldsymbol{x}$ is determined by $\sum_{i=1}^{B} b_i 2^{i-1}+1$. An example of natural mapping for 4PPM can be seen in Fig. 1(a).

B. Soft Demapping Q-ary PPM Symbols

For hard signal detection, we make a decision based on the slot with the maximum signal level [18]. As explained in Section IV, here we perform maximum *a posteriori*-based soft demodulation. According to Eq. (1), at the receiver, corresponding to a slot-word $\boldsymbol{x}$, we receive $\boldsymbol{r}=(r_1, r_2, \ldots, r_Q)$, where

$$r_i = x_i I + n_i, \quad i = 1, \ldots, Q. \tag{2}$$

x_i equals 0 or 1, depending on the mapped PPM symbol. Signals r_i are statistically independent according to the assumptions of Section III. For the sake of demonstration simplicity, let us consider the case of 4PPM. Remember the bit-symbol mapping illustrated in Fig. 1(a). The likelihood ratio (LR) on the bit b_1 is given by Eq. (3), where, for instance, $P(\boldsymbol{r}|b_1=1)$ is the probability density function of $\boldsymbol{r}$ conditioned to $b_1=1$:

$$\begin{aligned}\mathrm{LR}(b_1) &= \frac{P(\boldsymbol{r}|b_1=1)}{P(\boldsymbol{r}|b_1=1)} = \frac{P(\boldsymbol{r}|b_1=1,b_2=0)+P(\boldsymbol{r}|b_1=1,b_2=1)}{P(\boldsymbol{r}|b_1=0,b_2=0)+P(\boldsymbol{r}|b_1=0,b_2=1)} \\ &= \frac{P(\boldsymbol{r}|x_2=1,x_1=x_3=x_4=0)+P(\boldsymbol{r}|x_4=1,x_1=x_2=x_3=0)}{P(\boldsymbol{r}|x_1=1,x_2=x_3=x_4=0)+P(\boldsymbol{r}|x_3=1,x_1=x_2=x_4=0)}.\end{aligned} \tag{3}$$

Taking into account our iterative detection scheme, we should also make use of the *a priori* information at the demapper input. Let L_1 and L_2 denote the *a priori* LLRs on the bits b_1 and b_2, respectively. These are, in fact, extrinsic LLRs at the decoder output, calculated in the previous iteration. (Obviously, at the first iteration,

these *a priori* LLRs are set to zero.) Let us use the superscripts apost and ext to explicitly denote the *a posteriori* and extrinsic soft values, respectively. The *a posteriori* likelihood ratio LR on b_1 is given in Eq. (4):

$$\begin{aligned}\mathrm{LR}^{\mathrm{apost}}(b_1) &= \frac{\exp\left(\frac{-r_1^2}{2\sigma_n^2}+\frac{-(r_2-I)^2}{2\sigma_n^2}+\frac{-r_3^2}{2\sigma_n^2}+\frac{-r_4^2}{2\sigma_n^2}\right)e^{L_1}+\exp\left(\frac{-r_1^2}{2\sigma_n^2}+\frac{-r_2^2}{2\sigma_n^2}+\frac{-r_3^2}{2\sigma_n^2}+\frac{-(r_4-I)^2}{2\sigma_n^2}\right)e^{L_1+L_2}}{\exp\left(\frac{-(r_1-I)^2}{2\sigma_n^2}+\frac{-r_2^2}{2\sigma_n^2}+\frac{-r_3^2}{2\sigma_n^2}+\frac{-r_4^2}{2\sigma_n^2}\right)+\exp\left(\frac{-r_1^2}{2\sigma_n^2}+\frac{-r_2^2}{2\sigma_n^2}+\frac{-(r_3-I)^2}{2\sigma_n^2}+\frac{-r_4^2}{2\sigma_n^2}\right)e^{L_2}} \\ &= \frac{\exp\left(\frac{r_2 I}{\sigma_n^2}\right)e^{L_1}+\exp\left(\frac{r_4 I}{\sigma_n^2}\right)e^{(L_1+L_2)}}{\exp\left(\frac{r_1 I}{\sigma_n^2}\right)+\exp\left(\frac{r_3 I}{\sigma_n^2}\right)e^{L_2}}.\end{aligned} \tag{4}$$

The LLR on b_1 is obtained by taking the logarithm of Eq. (4). We use the approximation of $\log(e^m+e^n) \approx \max(m,n)$ to simplify the calculation of LLRs. Then, Eq. (4) simplifies to

$$\begin{aligned}\mathrm{LLR}^{\mathrm{apost}}(b_1) \approx &\max\left(\frac{r_2 I}{\sigma_n^2}+L_1,\frac{r_4 I}{\sigma_n^2}+L_1+L_2\right) \\ &-\max\left(\frac{r_1 I}{\sigma_n^2},\frac{r_3 I}{\sigma_n^2}+L_2\right).\end{aligned} \tag{5}$$

Remember that we have to provide extrinsic LLRs for the SISO decoder. Then,

$$\begin{aligned}\mathrm{LLR}^{\mathrm{ext}}(b_1) &= \mathrm{LLR}^{\mathrm{apost}}(b_1)-L_1 \\ &= \max\left(\frac{r_2 I}{\sigma_n^2},\frac{r_4 I}{\sigma_n^2}+L_2\right)-\max\left(\frac{r_1 I}{\sigma_n^2},\frac{r_3 I}{\sigma_n^2}+L_2\right).\end{aligned} \tag{6}$$

Similarly, the extrinsic LLR on b_2 is calculated as follows:

$$\mathrm{LLR}^{\mathrm{ext}}(b_2) = \max\left(\frac{r_3 I}{\sigma_n^2},\frac{r_4 I}{\sigma_n^2}+L_1\right)-\max\left(\frac{r_1 I}{\sigma_n^2},\frac{r_2 I}{\sigma_n^2}+L_1\right). \tag{7}$$

Checking Eqs. (6) and (7), we see that the extrinsic LLR on a bit does not depend on its *a priori* LLR. Generalization of the LLR calculation to the case of Q-ary PPM is considered in [34]; we do not reproduce it here because of space limitation. Notice that for the case of BPPM, as the demodulation is done bitwise, the iterative scheme cannot be used. However, a binary code is well adapted to this case.

VI. Extension to Multipulse PPM

For MPPM, an important issue is the bit-symbol mapping that can affect considerably the receiver performance. Investigating this point, we propose a mapping guideline for a general MPPM modulation scheme. Soft demapping, on the other hand, is similar to that explained for the monopulse QPPM in Subsection V.B.

A. MPPM Bit-Symbol Mapping

Consider the general case of w-QPPM. There are

$$C_w^Q = \binom{Q}{w}$$

possibilities of choosing w ON slots among Q. So, every MPPM symbol can represent up to $L=\log_2(C_w^Q)$ bits. However, C_w^Q may not be a power of two; so benefiting from the maximum L may require a complicated bit-symbol mapping [21]. Here, as a simple solution, we take the integer part of L as the number of bits per symbol B. Then, there are $P_{2^B}^{C_w^Q}$ possibilities for mapping bits from the set $\{b_B b_{B-1}\ldots b_1\}$ into symbols in the set $\{x_1 x_2 \ldots x_Q\}$. Let us consider the two cases of 2-4PPM and 2-8PPM in the following.

B. Case of 2-4PPM

With $w=2$ and $Q=4$, we have $L \simeq 2.58$, and we take $B=2$. There are $P_4^6=360$ different ways for mapping the bit set $(b_2 b_1)=\{00,01,10,11\}$ into a symbol set of size 4, among the 6 possible symbols {0011, 0101, 0110, 1001, 1010, 1100}. Note that the Hamming distance between any symbol pair equals either 2 or 4. Since the order matters in a bit-symbol mapping, we have to find the optimal mapping among these 360 possibilities. For this purpose, we first sort out these possibilities into $C_4^6=15$ symbol sets. Then, corresponding to each symbol set, there are $4!=24$ possibilities for bit-symbol mapping, which have the same average Hamming distance d, because permutations do not affect d. It can be easily verified that these 15

symbol sets can be divided into two groups that differ in d, one with $d=2.67$ and the other with $d=2.33$. (We have $C_2^3=3$ possibilities for the first group with $d=2.67$, and $C_1^3C_1^2C_1^2=12$ possibilities for the other with $d=2.33$.) Now, for each 24 possible bit-symbol mappings corresponding to a special symbol set, we furthermore specify the parameters d_1 and d_2, which are the average Hamming distances between two symbols (slot-words) differing in one and two bits in (b_2b_1), respectively. We have summarized in Table I the classification of different mappings, where we have specified d, d_1, and d_2 for different symbol sets together with the number of mappings corresponding to each set. We have also provided a mapping example at the right of each set in Table I. The second example, i.e., row two, "Best," is what we had already illustrated in Fig. 1(b).

The distances d, d_1, and d_2 are important parameters that affect the receiver performance. The most important parameter is d: a larger d results in general in a lower symbol error rate. The bit error rate (BER), on the other hand, also depends on d_1 and d_2.

In the case of noniterative detection, the more important parameter after d is d_2: to obtain better performance, we should first choose a mapping with the largest d, and then maximize, in descending priority order, d_2 and d_1. Things are a little different if we perform iterative detection. In fact, to optimize the mapping, after maximizing d, we should maximize, in descending priority order, d_1 and d_2. This concept is similar to the so called anti-Gray mapping, already investigated for RF communication systems employing iterative detection [35–38]. In particular, ten Brink in [36] studied, for different mappings, the bitwise mutual information (MI) on a bit, given the *a priori* knowledge of one or more bits. He showed that for a better performance improvement through iterations, this conditioned bitwise MI should be maximized. The anti-Gray mapping and the mapping method we proposed above satisfy this criterion.

From Table I, the mapping that we called "Best" is optimized by following this guideline. The performance comparison of the four mapping examples will be done in Subsection VII.D. Note that the mapping "Hell" does not work in an iterative scheme, although it has the largest d: if $b_1=1$, choice of $b_2=0$ or $b_2=1$ is equivalent to choosing between the possibility of $(x_1=0, x_2=1)$ or $(x_1=1, x_2=0)$, respectively. If $b_1=0$, choice of $b_2=0$ or $b_2=1$ is again equivalent to choosing between the possibility of $(x_1=0, x_2=1)$ or $(x_1=1, x_2=0)$, respectively. So, *a priori* information on b_1 does not help the detection of b_2 and vice versa. It can be easily verified that the extrinsic LLR for one bit does not depend on the *a priori* LLR on the other bit.

C. Case of 2-8PPM

Here, we have $L=\log_2(C_2^8)\simeq 4.8$ and so we can do the mapping by taking $B=3$ or $B=4$. Let us consider $B=3$, as it is the number of bits for the equivalent 8PPM modulation. There are P_8^{28} possibilities for mapping $(b_3b_2b_1)$ into $\boldsymbol{x}$ with two ON slots among $Q=8$. We verified that among the P_8^{28} possibilities, there are 14 groups of symbol sets that have different d. For simplicity, in Table II, we just consider two groups corresponding to the maximum and minimum d, i.e., 3.4 and 2.4, respectively. For each group, we have provided two bit-symbol mapping examples obtained by maximizing, in descending and ascending priority order, d_1, d_2, and d_3. We leave the performance comparison of these mappings to SubsectionVII.D.

Note, finally, that for the classic Q-ary PPM, we have $d=d_1=d_2=\cdots=2$ irrespective of the mapping. So, we have the same convergence property for any mapping.

VII. Numerical Results

Here we present some simulation results to study the performance of our proposed BCID scheme. The system performance is evaluated in terms of average BER as a function of signal-to-noise ratio (SNR). Electrical SNR is considered in the form of E_b/N_0, where E_b is the averaged received energy per information bit and N_0 is the noise unilateral power spectral density. In the following, we provide details of the simulation parameters.

TABLE I
Possible Bit-Symbol Mappings and Examples for 2-4PPM

No.ofSymbol Sets	No. of Possible Bit-Symbol Mappings	d	d_1	d_2	b_2b_1	0 0	0 1	1 0	1 1
3	$8\times3=24$	2.67	2	4	Hell	0101	0110	1001	1010
3	$16\times3=48$	2.67	3	2	Best	0101	1010	0011	1100
12	$8\times12=96$	2.33	2	3	Bad	0101	0011	1100	0110
12	$16\times12=192$	2.33	2.5	2	Good	0011	0101	1100	0110

TABLE II
MAPPING EXAMPLES FOR 2-8PPM

$b_3\ b_2\ b_1$	0 0 0	0 0 1	0 1 0	0 1 1	1 0 0	1 0 1	1 1 0	1 1 1	d	d_1	d_2	d_3
Best	11000000	00001010	00110000	00000101	00000011	01010000	00001100	10100000	3.4	4	3.3	2
Good	11000000	10100000	01010000	00110000	00001100	00000101	00001010	00000011	3.4	2.7	4	4
Bad	01100000	10001000	10000100	10010000	10000010	11000000	10000001	10100000	2.4	2.5	2.3	2
Worst	01100000	10100000	11000000	10001000	10000010	10000100	10000001	10010000	2.4	2.2	2.5	2.5

A. Simulation Parameters

We consider two cases of a channel without atmospheric turbulence that we call an AWGN channel (standing for additive white Gaussian noise) and a weak-turbulence channel. For the latter case, we set the Rytov variance χ^2 to 0.04, resulting in $\alpha=51.9$ and $\beta=49.1$ in the $\Gamma\Gamma$ model. To do a fair comparison between the performances of different modulations, we fix for all modulation schemes the information transmission rate that we denote R_b, as well as the average transmitted optical power, denoted P_{av}. Fixing this latter parameter is important because it controls the total optical energy consumption for the transmission of a given volume of data. Denoting the channel coding rate R_c, we further define the bit rate $R=R_b/R_c$, in contrast to the information rate R_b.

Taking fixed R_b and P_{av} into account, we set the transmitted beam intensity I_0 (in ON slots) for a given modulation. Considering the noise unilateral power spectral density N_0, we also have to set the receiver noise variance σ_n^2 according to the occupied bandwidth that we consider as $1/T$, where T is the slot duration. We specify below the calculation of I_0, σ_n^2, and E_b for different modulations that we will consider. Notice that we take R_c into account in the calculation of E_b.

- For OOK, we have $T=T_s=1/R$, and hence we set

$$I_0 = 2P_{\text{av}}, \quad \sigma_n^2 = \frac{N_0}{2}R, \quad E_b = \frac{2P_{\text{av}}^{\ 2}}{R_b}. \tag{8}$$

- For QPPM, we have $T_s=(\log_2 Q)/R$, $T=T_s/Q=\log_2 Q/QR$. We set

$$I_0 = QP_{\text{av}}, \quad \sigma_n^2 = \frac{N_0}{2}\frac{Q}{\log_2 Q}R, \quad E_b = \frac{QP_{\text{av}}^{\ 2}}{R_b}. \tag{9}$$

- For w-QPPM, with B bits per symbol, we have $T_s=B/R$ and $T=T_s/Q=B/QR$. Then,

$$I_0 = \frac{QP_{\text{av}}}{w}, \quad \sigma_n^2 = \frac{N_0}{2}\frac{Q}{B}R, \quad E_b = \frac{QP_{\text{av}}^{\ 2}}{wR_b}. \tag{10}$$

B. Performance of Classical Coding Methods

Let us begin by studying the performances of the classic existing methods. For this, we consider three coding schemes: Reed Solomon (RS) codes, simple binary convolutional codes, and binary TCs. For RS code, we consider (239, 255) and (127, 255) codes with coding rates of 0.94 and 0.5, respectively. As the convolutional code, we consider the rate 0.5 recursive systematic convolutional (RSC) code (1,5/7) of constraint length $K=3$, where the numbers 5 and 7 represent the code polynomial generators in octal [39]. For TC, we consider the parallel concatenation of two (1,5/7) RSC codes [40]. Note that we should set the same coding rate for different codings in order to perform a fair comparison between them. To obtain the same coding rate of 0.5 as the convolutional code, we perform homogeneous puncturing on the parity bits (see [8] for details). Also, three iterations are processed for turbo SOVA decoding, giving a near-convergence performance. Note that the use of more powerful codes (with larger K) provides negligible performance improvement in the presence of atmospheric turbulence.

We have contrasted the receiver performances for different modulation and coding schemes in Fig. 3. Each frame of symbols corresponds to about 2000 bits. Concerning modulation schemes, as expected, the performance of OOK is the same as BPPM (results are not shown in Fig. 3). Also, for QPPM, a better performance is obtained by increasing Q. Concerning coding

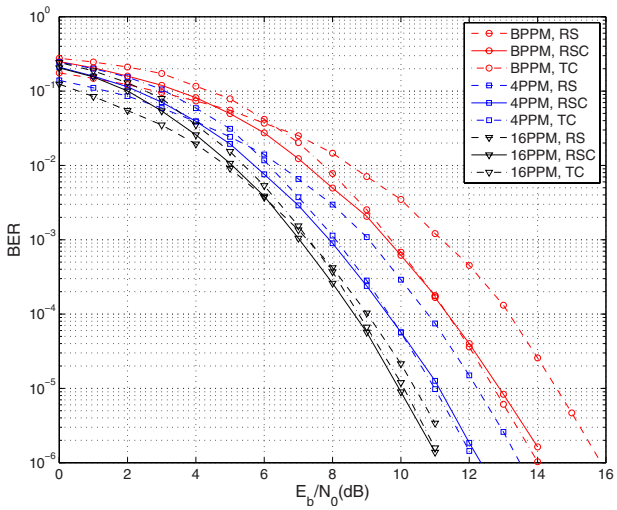

Fig. 3. (Color online) Comparison of different coding and modulation schemes, weak turbulence regime with $\chi^2=0.04$. RSC code, (1,5/7); RS code, (239,255); TC, punctured parallel concatenation of two RSC (1,5/7) codes.

schemes, interestingly, there is not a considerable difference between the performances of the convolutional and TC schemes. Also, for 16PPM, TC outperforms the convolutional code only for very low BER. It is the same for 8PPM (results are not shown). Concerning the RS code, unless for very high SNR (higher than the values in Fig. 3), the (127, 255) code has a poorer performance than the (239, 255) code, although this latter has a higher coding rate. For this reason, we preferred to present the curves for this latter scheme. [The (239, 255) RS code has been proposed in the DVB-S (digital video broadcasting–satellite) standard [41].] From Fig. 3, we see that the performances of convolutional and TC approach that of RS for increased Q. We deduce that for increased Q, these schemes lose their efficiency, because, as explained before, they are not adapted to nonbinary modulations.

C. Performance of BCID for Q-ary PPM

Consider now the proposed BCID scheme for QPPM. In the sequel, we always consider the (1,5/7) RSC the channel code.

1) Performance Over the AWGN Channel: Let us first consider the AWGN channel, i.e., without atmospheric turbulence. We have presented in Fig. 4 BER curves versus SNR corresponding to the first, second, and fifth iterations for the three cases of QPPM with $Q=4,8,16$. Full convergence is attained after about five iterations. As expected, the gain obtained by the iterative detector is specially significant for 8PPM and 16PPM modulations. For instance, for BER$=10^{-5}$, the SNR gain after full convergence is about 0.88, 1.61, and 2.25 dB for the cases of 4PPM, 8PPM, and 16PPM, respectively. The interesting point is that it is sufficient to process only two iterations at high enough SNR.

Remember that the role of the (de)interleaver is to decorrelate the LLRs input to the SISO decoder. The larger the interleaver size, the less correlated the LLRs. In Fig. 4, the interleaver size is about 2000 for 4PPM, 4000 for 8PPM, and 8000 for 16PPM. Negligible improvement is obtained for larger interleavers. By increasing the number of bits per symbol, we should increase the interleaver size because the outputs of the bit-level demapper are more correlated. Note that a larger interleaver implies a larger latency in data detection. For the sake of completeness, we have also shown in Fig. 4 for the case of 16PPM the BER floor curve that is obtained by feeding the demapper with perfect *a priori* LLRs.

2) Performance for a Weak Turbulence Regime: Consider now the case of a weak turbulence channel. We have presented the performance curves in Fig. 5 for the three previous modulation schemes. Other simulation parameters are the same as in Fig. 4. The SNR gain is again significant, and the convergence behavior through iterations is almost the same as for the AWGN channel. We notice an SNR gain of about 1.05, 1.35, and 1.4 dB for the cases of 4PPM, 8PPM, and 16PPM, respectively, at BER$=10^{-5}$ and after five receiver iterations. Note that curves corresponding to the first iteration are equivalent to those shown in Fig. 3.

3) Convergence Analysis of the Iterative Receiver: We use the EXIT (extrinsic information transfer) charts [42,43] to study the convergence of the receiver. Let us first present a brief introduction on this tool. EXIT charts are based on the flow of the extrinsic informa-

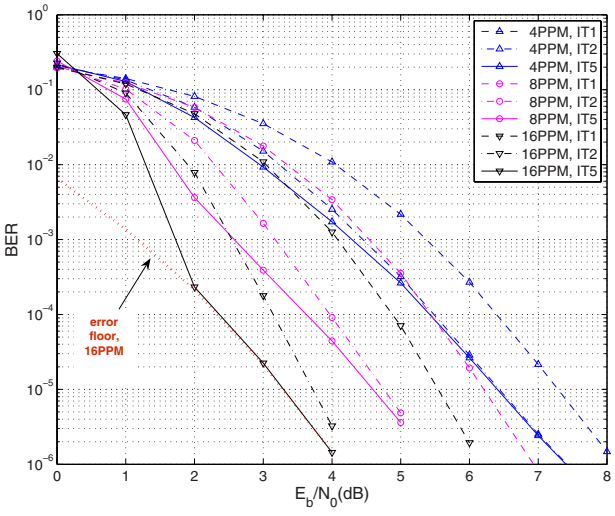

Fig. 4. (Color online) Performance of the iterative receiver for the AWGN channel, Q-ary PPM with $Q=4,8,16$, RSC (1,5/7) code; ITm denotes the mth iteration. Also shown is the error floor for the case of 16PPM.

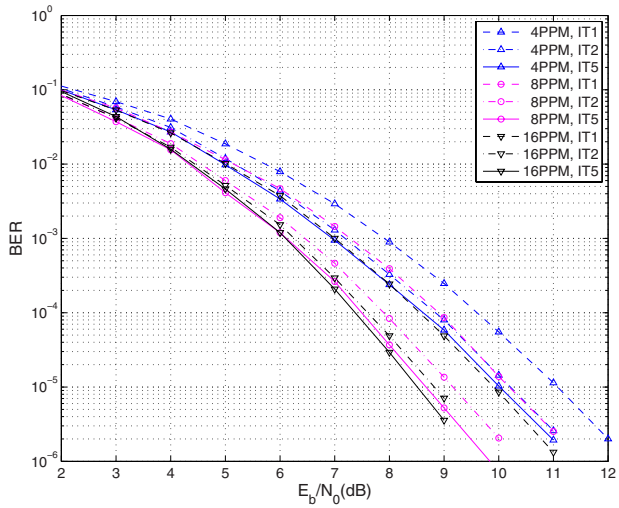

Fig. 5. (Color online) Performance of the iterative receiver for the weak turbulence channel with $\chi^2=0.04$, Q-ary PPM with $Q=4,8,16$, RSC (1,5/7) code; ITm denotes the mth iteration.

tion exchanged between the SISO blocks in an iterative scheme. By this method, the LLRs input to a SISO block are assumed to be uncorrelated and to follow a Gaussian distribution. Letting ξ denote the *a priori* LLRs and letting μ_ξ and σ_ξ^2 denote their mean and variance, respectively, we furthermore assume that $\mu_\xi=\sigma_\xi^2/2$, corresponding to a bit 1, and $\mu_\xi=-\sigma_\xi^2/2$, corresponding to a bit 0 [42]. Let I_A (subscript A indicates *a priori*) and I_E (subscript E indicates extrinsic) denote the mutual information (MI) at the input and output of a SISO block, respectively. The EXIT chart is considered the transfer function mapping the input information $I_A \in [0,1]$ to the output information $I_E \in [0,1]$. To obtain the EXIT curves, for each given I_A, we generate at the input of a SISO block, Gaussian distributed *a priori* LLRs with the appropriate variance. The MI I_E at the output of the module is then calculated by histogram estimation. The behavior of the iterative detector is determined by associating $I_E^{DEM} \Rightarrow I_A^{DEC}$, and inversely, $I_E^{DEC} \Rightarrow I_A^{DEM}$, where the superscripts DEM and DEC refer to the demapper and the channel decoder, respectively.

We have shown in Fig. 6 the EXIT chart of the SOVA decoder for RSC (1,5/7), as well as those of the demapper for the three modulations 4PPM, 8PPM, and 16PPM, at $E_b/N_0=4$ dB for the case of the AWGN channel. It is seen that the EXIT curve of 16PPM lies above that of 8PPM, and the latter lies above the EXIT curve of 4PPM. Note that the final BER depends on the intersection point of the EXIT curves of the demapper and the decoder. The closer the corresponding I_E^{DEC} is to 1, the lower the BER. The fact that a higher-order modulation gives a better BER performance is hence verified. We have also shown the trajectory describing the convergence of the receiver for 16PPM. We notice that about two iterations are sufficient to attain almost full convergence of the receiver. The convergence rate is almost the same for all these modulations, as the EXIT curves have almost the same slope. Note that the assumption of uncorrelated Gaussian *a priori* LLRs is not perfectly satisfied in practice. As a result, EXIT charts do not predict the convergence behavior of the receiver exactly. In other words, the obtained trajectory provides an asymptotic description of the receiver convergence.

D. Performance of BCID for MPPM

We consider the cases of 2-4PPM and 2-8PPM for which we discussed the bit-symbol mapping in Subsection VI.A. Note that, in general, there is more correlation between the bit-level LLRs at the demapper output for MPPM, compared with the equivalent PPM scheme, and a larger interleaver should be used. We use interleaver sizes of 4000 and 8000 for the cases of 2-4PPM and 2-8PPM

1) Case of 2-4PPM: We show in Fig. 7 the receiver BER performances for the four mappings already specified in Table I, for the case of the AWGN channel, as well as the corresponding curves for the mapping "Best" for the weak turbulence channel. First, consider the mapping "Best." It has the best performance after the receiver convergence, as it has the largest d and d_1 (see Table I and Subsection VI.A). We notice a more significant gain by iterative processing than what we had for a simple 4PPM (Figs. 4 and 5). The SNR gain at BER$=10^{-5}$ after five receiver iterations is about 1.86 and 1.7 dB for the cases of AWGN and weak turbulence channels, respectively. It is not a surprise that the overall performance is not better than

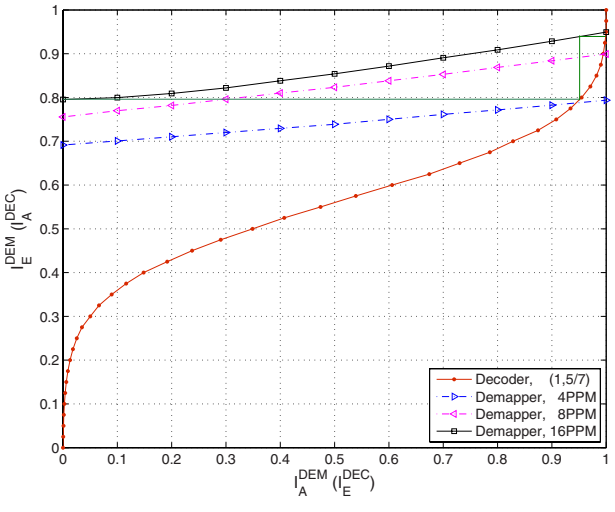

Fig. 6. (Color online) EXIT charts of the SOVA decoder [corresponding to the RSC code (1,5/7)] and the demapper for the three modulations 4PPM, 8PPM, and 16PPM, for $E_b/N_0=4$ dB and AWGN channel. The trajectory describing the receiver convergence for 16PPM is also shown.

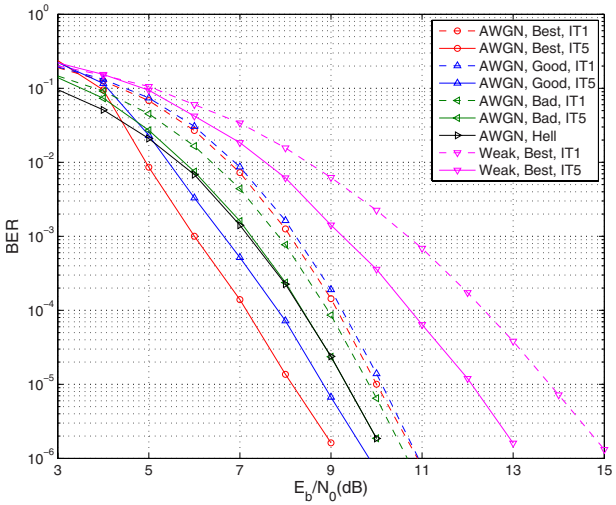

Fig. 7. (Color online) Performance of the iterative receiver for 2-4PPM modulation with $B=2$ for different mappings for the AWGN channel and the "Best" mapping for the weak turbulence channel. RSC (1,5/7) code; ITm denotes the mth iteration.

PPM; PPM remains more average-energy efficient and, hence, for a given E_b/N_0, it has a lower BER than MPPM. Considering the AWGN channel, the best performance in the first iteration is obtained for the mapping "Hell," for which we have the maximum d and d_2. Concerning the mappings "Good" and "Bad," which have the same d, better performance is obtained at the first iteration for the latter (which has a larger d_2), whereas after the convergence a lower BER is achieved for the former (which has a larger d_1). The same behavior is observed for the case of the weak turbulence channel (results are not shown).

These results are confirmed by EXIT charts. Figure 8 shows (dashed curves) the EXIT charts for different mappings for the AWGN channel at $E_b/N_0=8$ dB. We notice that, for instance, in the absence of *a priori* MI, i.e., at the first iteration, the demapper for "Bad" provides a higher output MI than for "Best." However, for relatively high *a priori* MI ($I_{\mathrm{A}}^{\mathrm{DEM}}>0.35$), we have a larger demapper output MI for the mapping "Best." The intersection with the EXIT curve of the decoder is at a higher $I_{\mathrm{E}}^{\mathrm{DEC}}$ and, as a result, the final BER is lower. This illustrates the famous trade-off between earlier turbo cliff and lower BER floor. We also notice that for "Hell" the demapper EXIT curve is horizontal and no evolution of MI is achieved through iterations.

2) Case of 2-8PPM: Remember that, here, we can do the mapping by taking $B=3$ or $B=4$. Let us first consider $B=3$ and the mapping examples provided in Table II. We have shown in Fig. 9 BER curves for the AWGN channel, as well as those of the mapping "Best" for the weak turbulence channel. It is verified that the mapping "Best" gives the best performance after convergence. The SNR gain at BER$=10^{-5}$ after five iterations is about 3.6 dB and 1.75 dB, for the AWGN and weak turbulence channels, respectively.

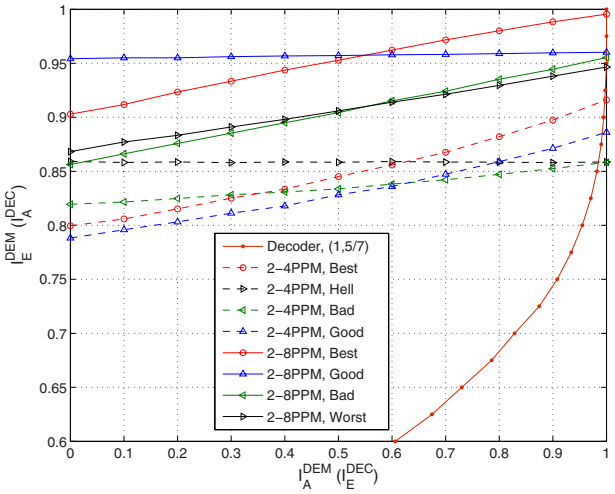

Fig. 8. (Color online) EXIT charts of the SOVA decoder and the demapper for the mappings in Tables I and II for 2-4PPM and 2-8PPM modulations. $E_b/N_0=8$ dB, AWGN channel.

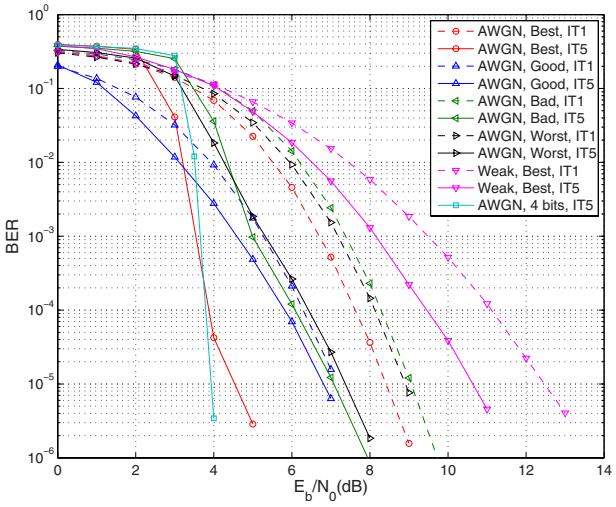

Fig. 9. (Color online) Performance of the iterative receiver for 2-8PPM modulation, $B=3$ for different mappings for the AWGN channel and "Best" mapping for the weak turbulence channel, as well as 2-8PPM with $B=4$ for AWGN channel. RSC (1,5/7) code; ITm denotes the mth iteration.

The corresponding EXIT charts are also shown in Fig. 8 (solid curves) for the AWGN channel at $E_b/N_0=8$ dB. The performance for different mappings can again be justified by considering the parameters d, d_1, d_2, and d_3 in Table II. We do not discuss them for the sake of brevity.

We have also presented in Fig. 9 the BER curve for 2-8PPM with $B=4$ for the AWGN channel and after five iterations. The corresponding mapping is optimized according to the proposed mapping guideline. Comparing with Fig. 4, we notice that interestingly, at low BER, this 2-8PPM scheme outperforms even the 16PPM (which has the same $B=4$), given that the slope of the BER curve after convergence is larger than that of 16PPM. So, overall, this 2-8PPM scheme is preferred to 16PPM, as its PAPR is four times lower and it has twice the bandwidth efficiency.

VIII. Conclusions

We considered in this paper a simple channel coding solution adapted to PPM, based on a binary convolutional code. At the receiver, iterative soft demodulation and channel decoding are performed. We showed that a significant performance improvement is obtained by using the proposed scheme, especially for increased modulation order. In particular, we also extended the BCID scheme to the case of MPPM and showed that the resulting performance improvement highly depends on the underlying bit-symbol mapping. We addressed a design rule to obtain optimal mappings adapted to the iterative detection scheme.

With an appropriate mapping, the performance improvement is, in general, more significant than the case of classic PPM.

ACKNOWLEDGMENTS

This work was supported in part by the French PACA (Provence-Alpes-Côte d'Azur) Regional Council. The authors wish to thank Frédéric Chazelet from Shaktiware Co., Marseille, France, for his fruitful discussions. Parts of this work were presented at the ConTEL Conference, 2009, Zagreb, Croatia, and the SPIE Optics+Photonics 2009, Free-Space Laser Communications Conference, San Diego, CA [34,44].

REFERENCES

[1] V. W. S. Chan, "Free-space optical communications," *J. Lightwave Technol.*, vol. 24, no. 12, pp. 4750–4762, Dec. 2006.

[2] S. Bloom, E. Korevaar, J. Schuster, and H. Willebrand, "Understanding the performance of free-space optics," *J. Opt. Netw.*, vol. 2, no. 6, pp. 178–200, Jan. 2003.

[3] D. Kedar and S. Arnon, "Urban optical wireless communication networks: the main challenges and possible solutions," *IEEE Commun. Mag.*, vol. 42, no. 5, pp. 2–7, May 2004.

[4] S. Hranilovic, *Wireless Optical Communication Systems*. New York, NY: Springer-Verlag, 2005.

[5] L. C. Andrews and R. L. Phillips, *Laser Beam Propagation through Random Media*, 2nd ed. Bellingham, WA: SPIE Press, 2005.

[6] M. Uysal, L. Jing, and Y. Meng, "Error rate performance analysis of coded free-space optical links over gamma-gamma atmospheric turbulence channels," *IEEE Trans. Wireless Commun.*, vol. 5, no. 6, pp. 1229–1233, June 2006.

[7] F. Xu, M. A. Khalighi, P. Caussé, and S. Bourennane, "Performance of coded time-diversity free-space optical links," in *2008 24th Biennial Symp. on Communications*, Kingston, Canada, June 24–26, 2008, pp. 146–149.

[8] F. Xu, M. A. Khalighi, P. Caussé, and S. Bourennane, "Channel coding and time-diversity for optical wireless links," *Opt. Express*, vol. 17, no. 2, pp. 872–887, Jan. 2009.

[9] M. A. Khalighi, N. Aitamer, N. Schwartz, and S. Bourennane, "Turbulence mitigation by aperture averaging in wireless optical systems," in *ConTEL 2009: The 10th Int. Conf. on Telecommunications*, Zagreb, Croatia, June 8–10, 2009, pp. 59–66.

[10] S. G. Wilson, M. Brandt-Pearce, Q. L. Cao, and M. Baedke, "Optical repetition MIMO transmission with multipulse PPM," *IEEE J. Sel. Areas Commun.*, vol. 23, no. 9, pp. 1901–1910, Sept. 2005.

[11] J. Hamkins and B. Moision, "Multipulse pulse-position modulation on discrete memoryless channels," Interplanetary Netw. Prog. Rep., no. 42–161, pp. 1–13, May 2005.

[12] B. Moision and J. Hamkins, "Coded modulation for the deep-space optical channel: serially concatenated pulse-position modulation," Interplanetary Netw. Prog. Rep., no. 42–161, pp. 1–25, May 2005.

[13] M. Cheng, M. Nakashima, B. Moision, and J. Hamkins, "Optimizations of a hardware decoder for deep-space optical communications," *IEEE Trans. Circuits Syst. I*, vol. 55, no. 2, pp. 644–658, March 2008.

[14] H. Hemmati, *Deep Space Optical Communications*. New York, NY: Wiley, 2006.

[15] J. Hamkins and B. Moision, "Selection of modulation and codes for deep space optical communications," *Proc. SPIE*, vol. 5338, pp. 123–130, Jan. 2004.

[16] F. S. Vetelino, C. Young, L. C. Andrews, and J. Recolons, "Aperture averaging effects on the probability density of irradiance fluctuations in moderate-to-strong turbulence," *Appl. Opt.*, vol. 46, no. 11, pp. 2099–2108, April 2007.

[17] A. D. Wyner, "Capacity and error exponent for the direct detection photon channel—Part II," *IEEE Trans. Inf. Theory*, vol. 34, no. 6, pp. 1462–1471, Nov. 1988.

[18] R. M. Gagliardi and S. Karp, *Optical Communications*, 2nd. ed. New York, NY: Wiley, 1995.

[19] S. G. Wilson, M. Brandt-Pearce, Q. Cao, and J. H. Leveque, "Free-space optical MIMO transmission with *Q*-ary PPM," *IEEE Trans. Commun.*, vol. 53, no. 8, pp. 1402–1412, Aug. 2005.

[20] H. Sugiyama and K. Nosu, "MPPM: a method for improving the band-utilization efficency in optical PPM," *J. Lightwave Technol.*, vol. 7, pp. 465–471, March 1989.

[21] M. K. Simon and V. A. Vilnrotter, "Performance analysis and tradeoffs for dual-pulse PPM on optical communication channels with direct detection," *IEEE Trans. Commun.*, vol. 52, no. 11, pp. 1969–1979, Nov. 2004.

[22] J. L. Massey, "Capacity, cutoff rate, and coding for a direct-detection optical channel," *IEEE Trans. Commun.*, vol. COM-29, pp. 1651–1621, Nov. 1981.

[23] E. Forestieri, R. Gangopadhyay, and G. Prati, "Performance of convolutional codes in a direct-detection optical PPM channel," *IEEE Trans. Commun.*, vol. 37, no. 12, pp. 1303–1317, Dec. 1989.

[24] J. Hamkins, "Performance of binary turbo-coded 256-ary pulse-position modulation," Telecommun. Mission Oper. Prog. Rep., no. 42–138, pp. 1–15, April–June 1999.

[25] S. S. Muhammad, T. Javornik, I. Jelovcan, E. Leitgeb, and Z. Ghassemlooy, "Comparison of hard-decision and soft-decision channel coded *M*-ary PPM performance over free space optical links," *Eur. Trans. Telecommun.* (to be published: advance publication Nov. 6, 2008).

[26] D. Divsalar, R. M. Gagliardi, and J. H. Yuen, "PPM performance for Reed–Solomon decoding over an optical-RF relay link," *IEEE Trans. Commun.*, vol. 32, pp. 302–305, March 1984.

[27] G. E. Atkin and K.-S. L. Fung, "Coded multipulse modulation in optical communication systems," *IEEE Trans. Commun.*, vol. 42, nos. 2, 3, 4, pp. 574–582, Feb.–April 1994.

[28] G. E. Atkin and H. P. Corrales, "Orthogonal convolutional coding for the PPM optical channel," *J. Lightwave Technol.*, vol. 7, no. 4, pp. 731–734, April 1989.

[29] C. Douillard, M. Jézéquel, C. Berrou, A. Picart, P. Didier, and A. Glavieux, "Iterative correction of intersymbol interference: turbo-equalization," *Eur. Trans. Telecommun.*, vol. 6, no. 5, pp. 507–511, Sept.–Oct. 1995.

[30] M. A. Khalighi and J. J. Boutros, "Semi-blind channel estimation using EM algorithm in iterative MIMO APP detectors," *IEEE Trans. Wireless Commun.*, vol. 5, no. 11, pp. 3165–3173, Nov. 2006.

[31] M. F. Barsoum, B. Moision, M. Fitz, D. Divsalar, and J. Hamkins, "Iterative coded pulse-position-modulation for deep-space optical communications," in *IEEE Information Theory Workshop, 2007. ITW '07*, pp. 66–71, Lake Tahoe, CA, Sept. 2–6, 2007.

[32] Y. Tan, J.-Z Guo, Y. Ai, W. Liu, and Y.-J. Fei, "A coded modulation scheme for deep-space optical communications," *IEEE Photon. Technol. Lett.*, vol. 20, no. 5, pp. 372–374, March 2008.

[33] Y. Tan, J.-Z Guo, and Y. Ai, "Iterative coded modulation with code rate flexibility for optical space communications," *IEEE Photon. Technol. Lett.*, vol. 21, no. 2, pp. 67–69, Jan. 2009.

[34] F. Xu, M. A. Khalighi, and S. Bourennane, "Pulse position modulation for FSO systems: capacity and channel coding," in *ConTEL 2009—10th Int. Conf. on Telecommunications*, Zagreb, Croatia, June 8–10, 2009, pp. 31–38.
[35] S. ten Brink, J. Speidel, and R.-H. Yan, "Iterative demapping and decoding for multilevel modulation," in *IEEE Global Telecommunications Conf., 1998. GLOBECOM 98. The Bridge to Global Integration*, vol. 1, Sydney, Australia, Nov. 8–12, 1998, pp. 579–584.
[36] S. ten Brink, "Designing iterative decoding schemes with the extrinsic information transfer charts," *AEU Int. J. Electron. Commun.*, vol. 54, no. 6, pp. 389–398, Nov. 2000.
[37] A. van Zelst, R. van Nee, and G. A. Awater, "Turbo-BLAST and its performance," *IEEE VTS 53rd Vehicular Technology Conf., 2001. VTC 2001 Spring*, Rhodes, Greece, May 6–9 2001, vol. 2, pp. 1282–1286.
[38] N. S. Muhammad and J. Speidel, "Joint optimization of signal constellation bit labeling for bit-interleaved coded modulation with iterative decoding," *IEEE Commun. Lett.*, vol. 9, no. 9, pp. 775–777, Sept. 2005.
[39] J. G. Proakis and M. Salehi, *Digital Communications*, 5th ed. Columbus, OH: McGraw Hill, 2008.
[40] C. Berrou and A. Glavieux, "Near optimum error correcting coding and decoding: turbo-codes," *IEEE Trans. Commun.*, vol. 44, no. 10, pp. 1261–1271, Oct. 1996.
[41] *Digital Video Broadcasting (DVB); Framing Structure, Channel Coding and Modulation for Digital Terrestrial Television*, ETSI EN 300 744 V1.5.1, European Standard (Telecommunications Series), Nov. 2004.
[42] S. ten Brink, "Convergence behavior of iteratively decoded parallel concatenated codes," *IEEE Trans. Commun.*, vol. 49, no. 10, pp. 1727–1737, Oct. 2001.
[43] M. Tuchler, R. Koetter, and A. C. Singer, "Turbo equalization: principles and new results," *IEEE Trans. Commun.*, vol. 50, no. 5, pp. 754–767, May 2002.
[44] F. Xu, M. A. Khalighi, and S. Bourennane, "Efficient channel coding for pulse position modulation in terrestrial FSO systems," *Proc. SPIE*, vol. 7464, paper 74640M, Aug. 2009.

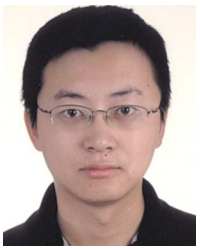

Fang Xu was born in 1983. He received his B.S. and M.S. degrees in Telecommunications from the University of Shanghai, Shanghai, China, and Lille University of Science and Technology, Lille, France, in 2004 and 2006, respectively. He also received his M.S. degree in Computer Science from Pierre and Marie Curie University, Paris, France, in 2007. He is now working toward his Ph.D. degree at the Institut Fresnel, Marseille, France. His research interests lie in free space optics (FSO) with an emphasis on signal processing. His doctoral research concerns atmospheric turbulence, channel coding, signal modulation, and diversity techniques.

Mohammad-Ali Khalighi (M'99, SM'07) received his B.Sc. and M.Sc. degrees in electrical engineering from Sharif University of Technology, Tehran, Iran, in 1995 and 1997, respectively, and his Ph.D. in electrical engineering (telecommunications) from Institut National Polytechnique de Grenoble (INPG), France, in 2002. From 2002 to 2005, he was with GIPSA-lab, Télécom Paris-Tech (ENST), and IETR-lab, as a Postdoctoral Research Fellow. He joined École Centrale Marseille and Institut Fresnel in 2005 as an Assistant Professor. His main research interests include coding, signal detection, and channel estimation for wireless communication systems.

Salah Bourennane received his Ph.D. degree from Institut National Polytechnique de Grenoble (INPG), France, in 1990 in signal processing. Currently, he is a Full Professor at École Centrale Marseille and he is the head of the Multidimensional Signal Processing team at Institut Fresnel, Marseille, France. His research interests include statistical signal processing, array processing, image processing, multidimensional signal processing, and telecommunications.